PNAS RESEARCH ARTICLE | SYSTEMS BIOLOGY

Nongenetic adaptation by collective migration

Lam Vo[a,b,1], Fotios Avgidis[a,b,c,1], Henry H. Mattingly[d,1], Karah Edmonds[a,b], Isabel Burger[a,b], Ravi Balasubramanian[a,b], Thomas S. Shimizu[c], Barbara I. Kazmierczak[e], and Thierry Emonet[a,b,f,2]

Affiliations are included on p. 10.

Edited by Victor Sourjik, Max-Planck-Institut fur terrestrische Mikrobiologie, Marburg, Germany; received November 14, 2024; accepted January 17, 2025 by Editorial Board Member Herbert Levine

Cell populations must adjust their phenotypic composition to adapt to changing environments. One adaptation strategy is to maintain distinct phenotypic subsets within the population and to modulate their relative abundances via gene regulation. Another strategy involves genetic mutations, which can be augmented by stress-response pathways. Here, we studied how a migrating bacterial population regulates its phenotypic distribution to traverse diverse environments. We generated isogenic *Escherichia coli* populations with varying distributions of swimming behaviors and observed their phenotype distributions during migration in liquid and porous environments. We found that the migrating populations became enriched with high-performing swimming phenotypes in each environment, allowing the populations to adapt without requiring mutations or gene regulation. This adaptation is dynamic and rapid, reversing in a few doubling times when migration ceases. By measuring the chemoreceptor abundance distributions during migration toward different attractants, we demonstrated that adaptation acts on multiple chemotaxis-related traits simultaneously. These measurements are consistent with a general mechanism in which adaptation results from a balance between cell growth generating diversity and collective migration eliminating underperforming phenotypes. Thus, collective migration enables cell populations with continuous, multidimensional phenotypes to flexibly and rapidly adapt their phenotypic composition to diverse environmental conditions.

collective behavior | non-genetic diversity | bacterial chemotaxis | population-level adaptation | microbial ecology

Significance

Conventional cell adaptation mechanisms, like gene regulation and stochastic phenotypic switching, act swiftly but are limited to a few traits, while mutation-driven adaptations unfold slowly. By quantifying phenotypic diversity during bacterial collective migration, we identified an adaptation mechanism that rapidly and reversibly adjusts multiple traits simultaneously. By balancing the generation of diversity through growth with the loss of phenotypes unable to keep up, this process tunes the phenotypic composition of migrating populations to the environments they traverse, without gene regulation or mutations. Given the prevalence of collective migration in microbes, cancers, and embryonic development, nongenetic adaptation through collective migration may be a universal mechanism for populations to navigate diverse environments, offering insights into broader applications across various fields.

Cell populations use various mechanisms to adapt their phenotypic distribution to new environments. One approach is to acquire mutations, such as in bacterial efflux pumps (1, 2) or the binding sites of EGFR (3) in cancer cells, to evade stressors. These processes typically occur over tens of generations (4–6). Another common approach is to regulate gene expression or switching between discrete phenotypic states (7, 8). A classic example of phenotypic switching is persister formation, where bacteria (9–11) or cancer cells (12) transition between antibiotic-resistant and chemotherapy-tolerant states (13, 14).

Here, we examined whether and how a migrating bacterial population regulates its phenotypic composition according to the environments it encounters. Groups of *Escherichia coli* cells collectively migrate by consuming attractant cues in their environment and chasing the traveling gradient that they create (15, 16). Individual cells with the same genotype exhibit varying tumble biases (TB) (Fig. 1*A*), chemoreceptor abundances (Fig. 1*B*), and other chemotaxis-relevant phenotypes, leading to differences in the speeds at which they climb the attractant gradients (17). These cells can travel together by spatially organizing within the migrating group such that their gradient-climbing abilities match the local steepness of the attractant gradient (15) (Fig. 1*C*). However, this spatial sorting mechanism is imperfect: Cells at the back, or the low performers, slowly fall behind the migrating population because the attractant concentration falls below the detection limit of their receptors (15). To maintain migration, the lost cells must be replaced through cell divisions (18, 19).

A recent theoretical model proposed that a dynamic balance between loss of low-performing phenotypes due to migration and production of new phenotypes by growth might be sufficient to adapt the population's composition to new environments (18). These two processes would balance out such that the traveling population becomes enriched with "fitter" phenotypes—those with higher chemotactic performance—increasing its expansion speed (15, 18). Since the demands of migration are different in different environments, which phenotypes are enriched should depend on the environment the population traverses (18) (Fig. 1*D*). This proposed mechanism does not require environment-dependent mutations or gene regulation. However, this model has never been experimentally tested.

Author contributions: L.V., F.A., H.H.M., T.S.S., B.I.K., and T.E. designed research; L.V., F.A., K.E., I.B., and R.B. performed research; L.V. and F.A. analyzed data; and L.V., F.A., H.H.M., T.S.S., B.I.K., and T.E. wrote the paper.

The authors declare no competing interest.

This article is a PNAS Direct Submission. V.S. is a guest editor invited by the Editorial Board.

[1]L.V., F.A., and H.H.M. contributed equally to this work.

[2]To whom correspondence may be addressed. Email: thierry.emonet@yale.edu.

This article contains supporting information online at https://www.pnas.org/lookup/suppl/doi:10.1073/pnas.2423774122/-/DCSupplemental.

Published February 19, 2025.

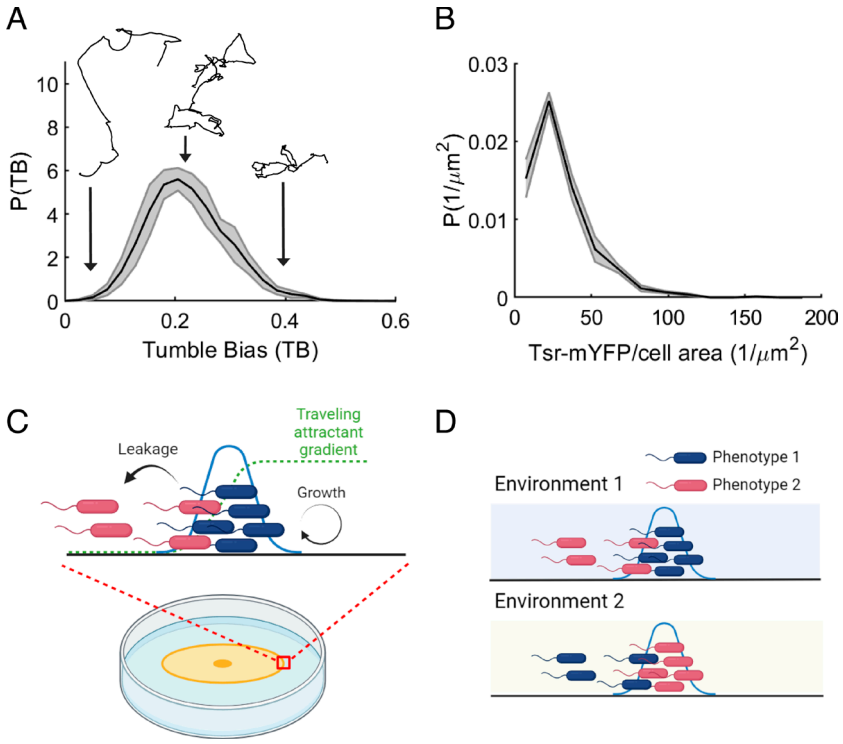

Fig. 1. Isogenic populations of bacteria exhibit diversity in behavioral and sensory phenotypes while performing collective migration. (*A*) In an isogenic population of *E. coli*, there is diversity in swimming behaviors, which can be quantified, for example, by measuring tumble bias in *Escherichia coli* RP437 (N_{rep} = 3, N_{cells} = 9,417). (*B*) There is also diversity in sensory ability, which correlates with variations in Tsr levels (as measured in *E. coli* MG1655, N_{rep} = 3, N_{cells} = 1,695). (*C*) Under nutrient-replete conditions, cells consume attractants and collectively migrate using the resulting traveling attractant gradients (20). During this process, cells spatially organize based on their ability to climb the traveling gradients (15). Cells with higher chemotactic performances lead at the front, while cells with lower chemotactic performances travel at the back and eventually fall behind the migrating group. In such nutrient-replete conditions, cells continue to divide and generate diversity by replenishing phenotypes. (*D*) Theory predicts (18) that the balance between environment-dependent cell loss and growth enables the migrating isogenic population to dynamically tune its phenotypic composition to the environments it traverses.

Here, we experimentally demonstrate this adaptation mechanism. By measuring the distribution of swimming behaviors and chemoreceptor abundances during migration in distinct environments, we observed that migrating *E. coli* populations tune their own distributions of chemotactic behaviors, without relying on gene regulation or mutations. Adaptation relies on the balance between the differential loss of low-performing phenotypes and the generation of diversity by growth during migration in each environment. The relaxation from the adapted distribution to the standing batch distribution occurs in approximately two generations. More broadly, migration and other collective behaviors when combined with growth may generally provide rapid and flexible ways for diverse populations to adapt to changing conditions.

Results

Collective Migration Tunes the Population's Distribution of Swimming Phenotypes. First, we investigated whether the TB distribution of an *E. coli* population can be adapted during collective migration with growth. Given that some swimming phenotypes are better at navigating than others (15, 17), we expected the TB distribution of a population, regardless of its starting point, to enrich for higher performing TBs during collective migration. To test this hypothesis, we compared the TB distributions of populations grown to exponential phase in batch cultures to those of populations migrating at constant speed on agarose swim plates containing excess nutrients. Excess nutrients ensure that cells in the migrating front are experiencing exponential growth (20, 21).

Populations with different batch TB distributions were generated by controlling the expression levels of the phosphatase CheZ using an inducible promoter in cells lacking the endogenous *cheZ* gene, as previously described (15, 22) (*Methods*). Growing this strain with a high concentration (16 ng/mL) or low concentration (2 ng/mL) of the inducer anhydrotetracycline (aTc) resulted in a population with low average TB or high average TB, respectively (*SI Appendix*, Fig. S1). The TB distribution of wild-type (WT) *E. coli* falls between these two extremes (Fig. 1*A*).

To propagate migrating waves of growing bacteria, we utilized the classic swim plate assay, in which cells migrate through a fibrous mesh of 0.14% w/v semisolid agarose supplemented with excess nutrients (16, 23). We inoculated *E. coli* populations with different batch TB distributions at the center of agarose swim plates, let them migrate for 15 h, collected cells at the edge of the expanding colonies ("wave"), and measured their TB distributions by transferring the cells to a liquid buffer and tracking single cells under a microscope. In parallel, we grew these same populations with identical inducer concentrations in shaking flasks ("batch") until exponential growth phase and measured their TB distributions (Fig. 2*A*). The inducer aTc degrades over time; therefore, we aged aTc before adding it to the batch culture growth medium to mimic the conditions in the migrating wave (*SI Appendix*, Fig. S2; *Methods*). The same experiments were performed with WT cells in the absence of aTc. By comparing the TB distributions of populations that had migrated on the plates with those propagated in batch culture, we quantified the effect of collective migration on the populations' TB distributions.

We found that the TB distribution of the high-TB population (batch mean TB = 0.31 ± 0.01, uncertainties throughout are the SE of the mean across biological replicates) shifted toward lower TBs (final mean TB = 0.23 ± 0.03) during migration on plates (Fig. 2 *E* and *H*). Conversely, the TB distribution of the low-TB population

(batch mean TB = 0.10 ± 0.01) shifted to higher TBs (final mean TB = 0.18 ± 0.01) after migration on the plates (Fig. 2 *C* and *F*). In both cases, the populations became enriched for cells with intermediate TBs of ~0.2, close to the mean TB of WT populations grown in batch culture (mean TB = 0.22 ± 0.03) (*SI Appendix*, Fig. S3). Consistent with these observations, the TB distribution of the migrating WT population (final mean TB = 0.22 ± 0.01) was similar to its batch culture distribution (Fig. 2 *D* and *G*). All changes in the mean TB during migration were statistically significant, as measured by the two-sided t test, except that of the WT population. Samples harvested 1 cm behind the migrating populations were marginally enriched for the low-performing TBs, though the effect was not significant, possibly because growth also occurred between the moment when these cells fell behind and when they were harvested (*SI Appendix*, Fig. S4).

To quantify how these shifts in phenotype composition affected migration speed, we measured the expansion radius of the migrating waves of the three populations on agarose swim plates over time and calculated the steady-state expansion speed using the slope of the linear part of the expansion radius profile (*Methods*; Fig. 2*B* and *SI Appendix*, Fig. S5). Early time points in migration could not be measured because the ring was not clearly visible. We found that the CheZ mutants reached their steady state speeds much later than the WT, possibly due to the scarcity of high-performing phenotypes in the batch culture distributions. However, once the CheZ mutants reached steady state, their migration speeds were close to that of the WT, illustrating the effectiveness of the adaptation mechanism. In particular, the WT population (mean steady-state expansion speed 0.174 ± 0.007 mm/min) and the high-TB population (0.170 ± 0.02 mm/min) expanded the fastest (difference in speed was not

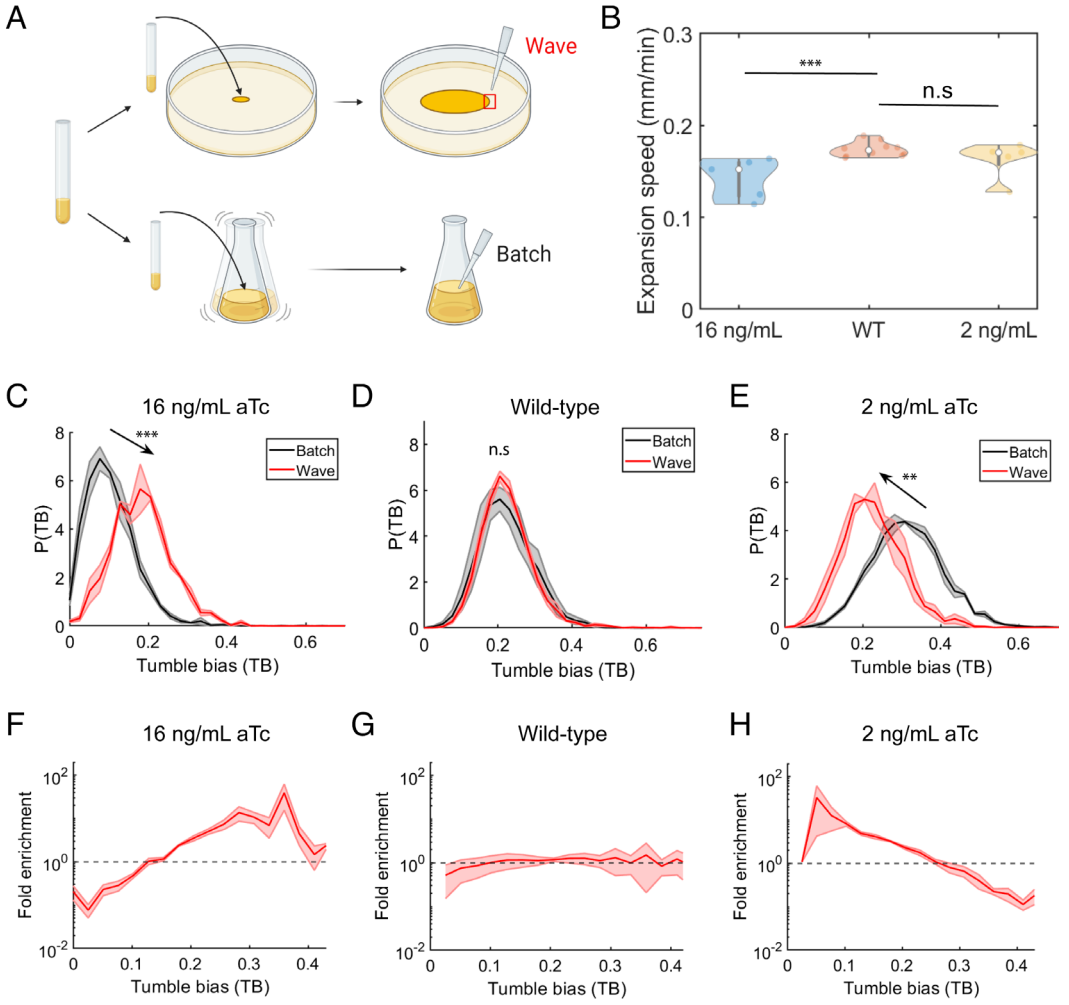

Fig. 2. Migration in agarose swim plate tunes TB distribution of the population: (*A*) Experimental design: a swim plate and shaking flask containing the same amount of inducer are inoculated with the same initial population. TB distributions are measured and compared between batch and the migrating ring ("wave") after spending the same amount of time in either condition. (*B*) Expansion speeds of RP437 wild-type (WT) (mean expansion speed 0.174 ± 0.007 mm/min; uncertainties throughout the paper are the SE of the mean across replicates; here, N_{rep} = 12, *ΔcheZ* (pTet-CheZ) induced with 2 ng/mL aTc (mean 0.170 ± 0.02 mm/min; N_{rep} = 6), and 16 ng/mL (mean 0.150 ± 0.02 mm/min; N_{rep} = 6) populations on agarose swim plates. The expansion radius over time was measured laterally and in one direction from the center to the edge of the migrating colony. Two-sided t-tests were performed throughout the text to determine significance of the difference between pairs of means (throughout, ***$P < 0.0005$, **$P < 0.005$, *$P < 0.05$, and n.s. = not significant). (*C*) Populations with low initial mean TB (mean TB = 0.10 ± 0.01; N_{rep} = 3, N_{cells} = 21,891) shift toward a higher mean TB after migration on the plates (0.18 ± 0.01; N_{rep} = 3, N_{cells} = 5,103). Shaded area on the TB distribution is the SEM probability in each TB bin. Significance here and throughout the figures refers to change in the mean of the distribution. (*D*) There was minimal or no shift in WT population's TB distribution during collective migration on the plates (0.22 ± 0.01; N_{rep} = 3, N_{cells} = 15,774) compared to batch culture (0.22 ± 0.03; N_{rep} = 3, N_{cells} = 9,417). (*E*) On the other hand, populations with high initial mean TB (0.31 ± 0.01; N_{rep} = 3, N_{cells} = 26,254) shifted toward a lower mean TB after migration (0.23 ± 0.03; N_{rep} = 3, N_{cells} = 6,951). (*F*) When low-TB populations migrated on the plates, fold enrichment of cells with high TB is observed, while cells with low TB are filtered out (N_{rep} = 3). Shaded area on the fold-enrichment throughout is the SE of the mean enrichment values within each TB bin (*G*). No enrichment and filtering of TB were observed in WT populations (N_{rep} = 3). (*H*) When high-TB populations migrated on the plates, enrichment of cells with low TB is observed, while cells with high TB are filtered out (N_{rep} = 3).

statistically significant). The low-TB population was slower (0.150 ± 0.02 mm/min; significant to $P < 0.005$), possibly due to the presence of very low-TB cells in the adapted population (*SI Appendix*, Fig. S3). The growth rates of WT, low-TB, and high-TB populations were similar (*SI Appendix*, Fig. S6), therefore differences in the steady-state expansion speeds were solely due to differences in chemotactic performance. Thus, migrating populations become enriched with high-performing phenotypes, increasing migration speed. In this environment, cells with TB close to 0.22 appear to perform best, which coincides with the average TB of the WT population in batch culture (*SI Appendix*, Fig. S3).

Tuning of Swimming Phenotype Distributions Is Nongenetic and Occurs Without Changes in *cheYZ* Expression. What mechanism enables a migrating bacterial population to tune its TB distribution? Our recent theory predicts that the tuning of phenotypic distributions is a dynamic, nongenetic process mediated by the loss of low-performing chemotaxis phenotypes (15) and production of new phenotypes through growth (18, 24, 25). However, during our swim plate assays, cells in the migrating populations could potentially acquire mutations that permanently altered their swimming behaviors (4–6). If TB tuning was nongenetic, then we expected that the TB distributions of cells in the migrating waves would revert to their standing TB distributions when grown in batch culture.

To distinguish between these possibilities, we isolated cells from the edge of the low- and high-TB migrating colonies on agarose swim plates, inoculated them into batch cultures with aTc, and measured their TB distributions after growth (Fig. 3*A*). The TB distributions of the migrating populations relaxed to their standing TB distributions after regrowth in batch culture, suggesting that the cells in the migrating population did not acquire mutations that permanently altered their swimming behaviors (Fig. 3 *B* and *C*).

Even without mutations, the observed shifts in TB distribution during migration could have been due to changes in gene expression. Chemotaxis is regulated during *E. coli* growth, leading to changes in a population's TB distribution at different growth phases (24). We verified that, in our conditions, TB and tumble frequency (TF) did not vary during steady, exponential growth phase (*SI Appendix*, Fig. S7 and *Discussion* therein). Still, if cells experienced different growth conditions as they migrated, expression of the response regulator CheY and its phosphatase CheZ could be affected, thus changing TB (15, 17). Given that there was excess nutrient on the plates, we expected that bacteria would remain in exponential phase for the duration of the experiment, and therefore that *cheY* and *cheZ* regulation would be constant throughout the plate as the population migrates. We measured the protein expression levels of CheY and CheZ by fusing them to fluorescent proteins (RFP and YFP, respectively) at their native chromosomal loci in a nonmotile strain. This nonmotile strain acted as a biosensor for detecting in vivo changes in *cheYZ* expression. We spread these cells uniformly on agarose swim plates, initiated migrating waves of motile, unlabeled WT cells at the center of the plates, and then picked cells from both the center and the edge of the migrating colonies (*Methods*). Fluorescent microscopy measurements (*Methods*) revealed no significant differences in CheY and CheZ levels between cells sampled from the center vs. the edge (*SI Appendix*, Fig. S8). This indicated that the expression of *cheY* and *cheZ* remains constant across the entire plate even as the wave migrates. We confirmed that migrating populations did not experience catabolite repression (26, 27) during the period of our measurements since catabolite repression effects only appeared at much longer times (*SI Appendix*, Fig. S9).

Together, these observations indicated that the adaptation of TB distributions was highly unlikely to be mediated by mutations or gene regulation.

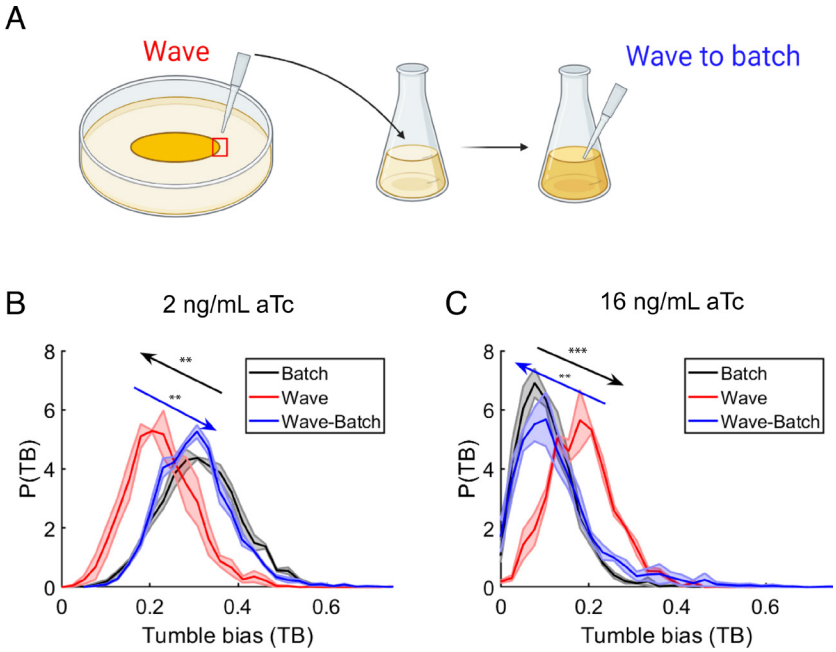

Fig. 3. Tuning of TB by collective migration is reversible. (*A*) To determine whether the tuning of TB becomes fixed or remains adaptable, we isolated cells from the edge of the migrating colonies ("wave"), grew the cells in liquid batch culture until exponential phase, and measured the TB distributions after growth ("wave-batch"). (*B*) Black and red are the TB distributions of populations with high initial TB before and after migrating on agarose swim plates (data replotted from Fig. 2*E*). Blue: TB distribution of cells that migrated (red) after regrowth in batch culture (mean TB = 0.30 ± 0.01; $N_{rep} = 3, N_{cells} = 15,774$). The TB distributions of the populations that migrated on agarose swim plates, after growing in flasks, shifted back to the original batch culture's distributions. (*C*) Similar to *B*, the TB distributions of populations with low initial TB, after growing in flask (blue; 0.13 ± 0.02; $N_{rep} = 3, N_{cells} = 20,403$), shifted back to the TB distributions observed in batch culture (black and red distributions are replotted from Fig. 2*C*). The mean values of "batch" and "wave-batch" TB distributions in both cases are not significantly different.

Tuning of Swimming Phenotype Distributions Adapts the Population to the Physical Environment. We have demonstrated that migrating cell populations nongenetically tune their own phenotypic composition, enriching the population for high-performing chemotaxis phenotypes. Since the performance of chemotaxis phenotypes varies in different environments (18), we expected that the TB distribution during migration would depend on the environment that the population traversed. Whereas cells need to tumble to escape traps in semisolid agarose (18, 23, 28), past work has shown that cells with low TB climb chemical gradients faster in liquid (17, 29). This suggests that the highest-performing phenotype in liquid has a lower TB than that in semisolid agarose, and thus migrating populations would enrich for lower TBs in liquid than in agarose.

To test this, we measured the TB distributions of migrating populations after traveling through a liquid environment (Fig. 4*A*). We again generated populations of *E. coli* with low and high average TBs and propagated migrating waves with these populations, as well as the WT, in capillary tubes filled with liquid media for 9 h. aTc was preaged so that the total aging time at the end of the capillary experiments was the same as in our agarose swim plate experiments. We then isolated cells from the migrating populations and measured their TB distributions after migration.

The WT population's TB distribution (batch mean TB = 0.22 ± 0.03) shifted to lower TB (final mean TB = 0.18 ± 0.01) during collective migration in liquid (Fig. 4 *D* and *G*). Low-TB cells were enriched up to a factor of 10, whereas high-TB cells were filtered out. When the population with high TB (batch mean TB = 0.31 ± 0.01) traveled through capillary tubes, its TB distribution shifted lower than it did when traveling on agarose swim plates (final mean TB = 0.16 ± 0.01) (Fig. 4*E*). The enrichment

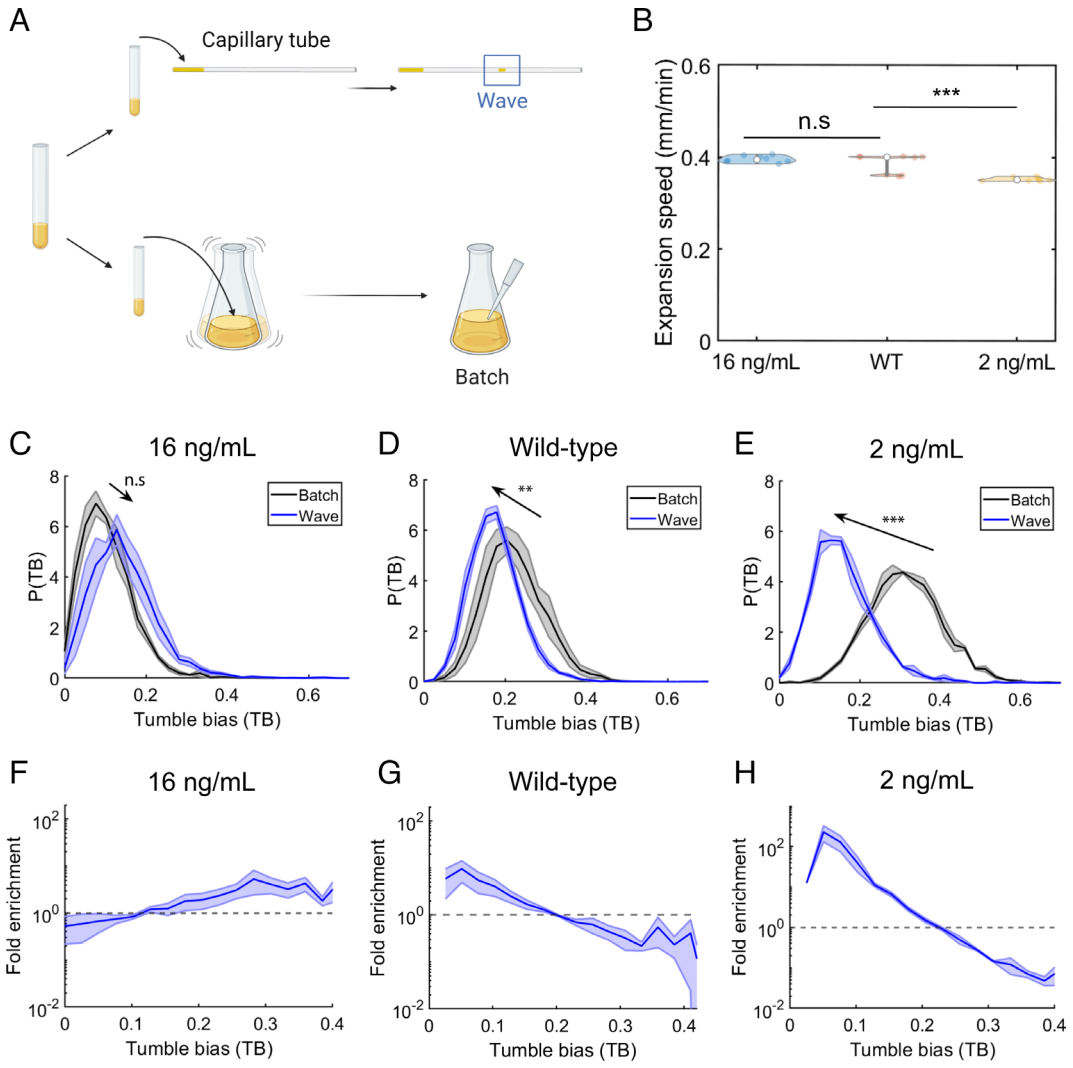

Fig. 4. Tuning of TB distribution is different in liquid environment: (*A*) Experimental design: A capillary tube and shaking flask containing the same amount of inducer are inoculated with the same initial population. TB distributions are measured and compared between batch and the migrating cells ("wave"). (*B*) Expansion speeds of RP437 WT (mean 0.386 ± 0.01 mm/min; N_{rep} = 9, *ΔcheZ* (pTet-CheZ) induced with 2 ng/mL aTc (mean 0.353 ± 0.001 mm/min; N_{rep} = 9), and 16 ng/mL aTc (0.396 ± 0.003 mm/min; N_{rep} = 9) populations in capillary tubes. (*C*) In liquid, populations with low initial mean TB (mean TB = 0.10 ± 0.01; N_{rep} = 3, N_{cells} = 21, 891) shift toward a higher mean TB (0.15 ± 0.03; N_{rep} = 3, N_{cells} = 20, 403), but which is slightly lower than the mean TB in agarose swim plates (0.18 ± 0.01, as in Fig. 2*C*). (*D*) Unlike in agarose swim plates, WT population's TB distribution (0.22 ± 0.03; N_{rep} = 3, N_{cells} = 9, 417) shifted toward a lower mean TB during collective migration in capillary tubes (0.18 ± 0.01; N_{rep} = 3, N_{cells} = 16, 768). (*E*) Populations with high initial mean TB (0.31 ± 0.01; N_{rep} = 3, N_{cells} = 26, 254) shifted toward a lower mean TB (0.16 ± 0.01; N_{rep} = 3, N_{cells} = 13, 434). The mean TB value is lower than what was observed during migration on agarose swim plates (0.23 ± 0.03, as in Fig. 2*D*). (*F*) For the migration of low-TB populations, the fold enrichment is smaller than in agarose swim plates. (N_{rep} = 3) (*G*). WT populations migrating in capillary tubes were enriched for low-TB cells (N_{rep} = 3), unlike what we observed when they migrated on agarose. (*H*) For high-TB populations, fold enrichment was stronger in capillary tubes compared to migration in agarose swim plates (N_{rep} = 3). More low-TB cells are enriched during migration in capillary tubes than on agarose plates.

of low-TB cells and filtering out of high-TB cells were much stronger in the capillary tubes (Fig. 4*H*) compared to the agarose swim plates (Fig. 2*H*). The TB distributions of the low-TB population (batch mean TB = 0.10 ± 0.01) shifted to a slightly higher mean TB when traveling through capillary tubes (final mean TB = 0.15 ± 0.03), but the shift was not statistically significant (Fig. 4*C*). In this case, the enrichment of high-TB cells and filtering out of low-TB cells was weaker in the capillary tubes (Fig. 4*F*) compared to agarose swim plates (Fig. 2*F*).

As in agarose, the position of migrating waves in capillary tubes increased linearly after they had propagated a few centimeters, indicating that their expansion speeds had reached steady state at the time we measured TB (*SI Appendix*, Fig. S10). Adaptation enabled the CheZ mutants and WT population to reach similar steady state migration speeds. The low-TB population had the fastest expansion speed (mean expansion speed 0.396 ± 0.003 mm/min). Its TB distribution shifted the least during migration in capillary tubes, suggesting that its standing TB distribution was better adapted for migration in liquid than the WT and high-TB populations (*Methods*; Fig. 4*B*). The expansion speed of the WT population was statistically indistinguishable from this (0.386 ± 0.01 mm/min). Finally, the high-TB population expanded slower than the other two populations (0.353 ± 0.001 mm/min).

Together, these results established that shifts in TB distribution during collective migration of *E. coli* enriched for phenotypes with highest chemotaxis performance in the environment being traversed.

We also tested whether environment-dependent adaptation of TB distributions by collective migration occurred in other WT *E. coli* strains, including: 1) HE205, a NCM3722 derivative from the Cremer and Hwa labs (20), 2) AW405, a K-12 strain originated from the Berg lab (23), 3) MG1655, a common K-12 lab strain (30), and 4) TW09231, or *Escherichia sp.* TW09231, a wild isolate from Lake Michigan (31). In all cases, migration in liquid resulted in populations enriched with lower TB cells than when migrating in agarose (*SI Appendix*, Fig. S11), consistent with adaptation by collective migration. These results demonstrate environment-dependent tuning of TB distributions across a wide range of both lab *E. coli* strains and a wild isolate, highlighting the universality of this adaptation mechanism.

Adapted TB Distribution Rapidly Relaxes Back to Batch Distribution. How quickly does the adapted phenotypic distributions of a migrating population reverse back to the standing batch distribution? To quantify this, *E. coli* populations were isolated from capillary tube assays and reinoculated into batch cultures. TB distributions were measured every 15 to 30 min throughout the growth period (Fig. 5*A*). We fitted the mean TB values over time to an exponential model to determine the characteristic timescale on which the mean TB returns to the level observed in batch culture (*Methods*). For WT RP437, it took about 2 doubling times for the TB distributions to return to those observed in batch cultures (Fig. 5*B*). The relaxation time scale of the mean was $\tau = 65.2 \pm 1.6$ min and the doubling time was 68.8 ± 1.5 min. The result was similar for an *E. coli* strain with slower growth rate, HE205. Its TB distribution also relaxed within approximately 2 doubling times (Fig. 5*C*). The relaxation time scale of the mean was $\tau = 106.1 \pm 6.3$ min and the doubling time was 92.3 ± 3.4 min. These results demonstrate that adaptation by collective migration is rapidly reversible, requiring only a few generations of growth.

Collective Migration Tunes the Population's Distribution of Sensing Phenotypes to Adapt to the Chemical Environment. Numerous phenotypic traits, in addition to tumble bias, affect a bacterium's chemotactic performance. One such trait is the cell's sensing capability, which correlates with the abundances of its chemoreceptors (32, 33). *E. coli* express five chemoreceptor species, of which ~90% are either Tar, which binds preferentially to L-aspartate, or Tsr, which binds preferentially to L-serine (34–36). Notably, Tsr is expressed separately from the chemotaxis

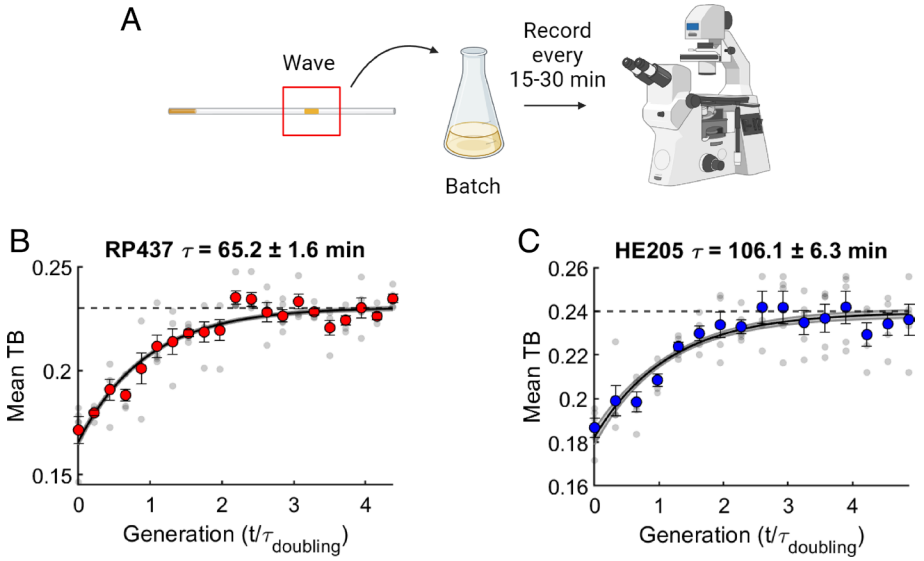

Fig. 5. Adapted TB distribution relaxes back to the standing batch distributions within a few generations. (*A*) Experimental design: *E. coli* RP437 and HE205 populations were inoculated in capillary tubes and let to migrate for 9 h. Migrating populations were isolated and grown in batch cultures. TB measurements were taken from the batch culture over the course of growth every 15 min (RP437) or 30 min (HE205). (*B*) In ~2 generations (growth rate = 0.604 ± 0.01 h^{-1}; $\tau_{doubling}$ = 68.8 ± 1.5 min; errors are the SE of the mean growth rates and doubling times; $N_{rep} = 3$), the mean TB of migrating populations returns back to the mean TB of populations observed in batch culture (the mean TB of the batch culture is represented as a horizontal dashed line). The gray dots are the mean TB of individual biological replicates. The red dots are the means across replicates (calculated from more than 30,844 trajectories for each time points; $N_{rep} = 5$), and the error bars are the SE of the mean. The means and SE across replicates were fitted with an exponential model, and a characteristic relaxation timescale τ and its error were determined using maximum likelihood estimation (*Methods*). The black line is the model fit, and the shaded area is the SD of the model. τ for RP437 is 62.5 ± 1.6 min—the error is the SD of the estimated τ. (*C*) Same as *B*, but for HE205. The blue dots are the means across replicates (calculated from more than 5,920 trajectories each time points; $N_{rep} = 5$). It takes ~2 generations (growth rate = 0.45 ± 0.01 h^{-1}; $\tau_{doubling}$ = 92.3 ± 3.4 min; $N_{rep} = 3$) for the TB distributions to relax back to the batch culture. τ for HE205 is 106.1 ± 6.3 min.

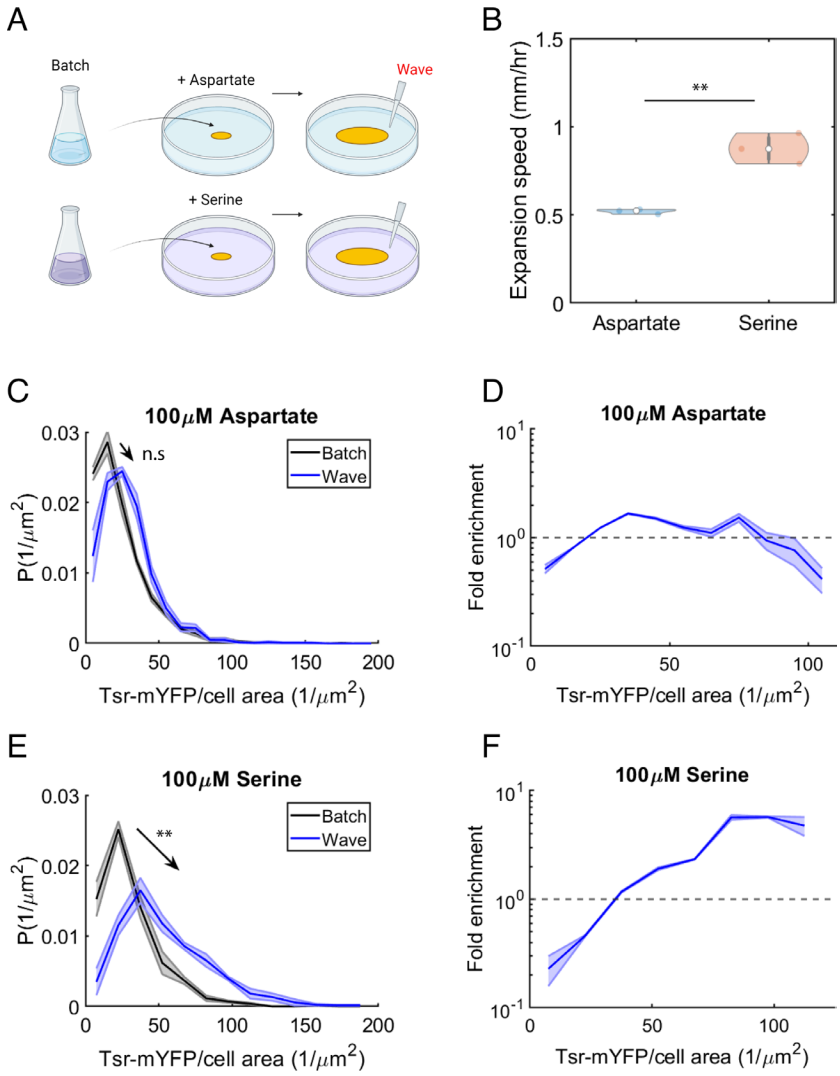

Fig. 6. Collective migration tunes the chemoreceptor levels depending on the attractants. (*A*) Experimental design: *E. coli* MG1655 WT with YFP-labeled Tsr was inoculated on swim plates supplemented with 100 μM aspartate or 100 μM serine. The fluorescence of single cells was measured in populations at the edge of the migrating colonies ("wave") and in populations growing in batch culture. The single-cell fluorescence divided by the cell area is used as a proxy for receptor concentration. (*B*) The expansion speeds of the migrating populations in agarose swim plates supplemented with 100 μM aspartate (0.52 ± 0.1 mm/h; $N_{rep} = 3$) or 100 μM serine (0.88 ± 0.05 mm/h; $N_{rep} = 3$). (*C*) Black is the distribution of Tsr levels of populations grown in batch culture with added aspartate (mean Tsr intensity = 23.7 ± 0.4 μm^{-2}; $N_{rep} = 3, N_{cells} = 2,076$), and blue is the distribution of Tsr levels of the migrating populations that chased aspartate (27.2 ± 3.8 μm^{-2}; $N_{rep} = 3, N_{cells} = 1,617$). Shaded areas on the Tsr intensity distributions are the SE of the mean probabilities in each bin of intensity value. (*D*) When chasing aspartate, the distributions of Tsr levels in migrating populations remained close to that in batch cultures, with only a weak fold increase in cells with intermediate Tsr levels and a weak fold decrease in cells with high Tsr levels. Shaded area on the fold-enrichment throughout is the SE of the mean enrichment values within each bin of Tsr intensity value. (*E*) Black is the distribution of Tsr levels of populations grown in batch culture with added serine (29.6 ± 2.9 μm^{-2}; $N_{rep} = 3, N_{cells} = 1,695$), and blue is the distribution of Tsr levels of the migrating populations that chased serine (53.6 ± 6.5 μm^{-2}; $N_{rep} = 3, N_{cells} = 675$). (*F*) During collective migration on swim plates supplemented with serine, there was a strong enrichment of cells with higher Tsr levels, while cells with lower Tsr levels were filtered out.

operon—which includes, among other genes, Tar, CheY, and CheZ (37)—allowing its abundance to vary independently of other chemotaxis genes affecting chemotaxis performance. Therefore, we predicted that Tsr could be enriched in a migrating wave that chases its cognate ligand L-serine.

We measured the Tsr protein expression levels in populations of *E. coli* migrating on agarose swim plates with 100 μM L-aspartate or 100 μM L-serine as attractants, and no other amino acids (Fig. 6*A*). As a carbon source, we used glycerol because it is not an attractant (38). To measure single-cell Tsr levels, we fused *tsr* on its native locus with mYFP (*Methods*). We used MG1655 as the parent strain here because, unlike RP437 (37, 39), it is not restricted by auxotrophic limitation and can grow in minimal media in the absence of amino acids. The expansion speed of the population was faster in serine (0.88 ± 0.05 mm/h) than in aspartate (0.52 ± 0.1 mm/h) (Fig. 6*B*) consistent with previous reports (20).

We compared the average mYFP fluorescence in single cells picked from the edge of the migrating colonies versus those grown in batch cultures supplemented with the same concentration of either L-aspartate or L-serine (*Methods*). When aspartate was the chemoattractant, distributions of Tsr levels within the migrating populations on swim plates were similar to those grown in batch cultures, with the mean Tsr level statistically indistinguishable from batch culture (Fig. 6*C*; mean intensities $\langle \mathrm{Tsr} \rangle_{\mathrm{batch}} = 23.7 \pm 0.4 \mu m^{-2}$ and $\langle \mathrm{Tsr} \rangle_{\mathrm{wave}} = 27.2 \pm 3.8 \mu m^{-2}$). We observed a slight enrichment of intermediate Tsr levels (Fig. 6*D*), possibly because of the assistance Tsr provides to the adaptation of Tar (CheR and CheB can methylate and demethylate neighboring Tar receptors when bound to the pentapeptide of Tsr) (40, 41). In contrast, collective migration led to strong enrichment for cells with high levels of Tsr when the population chased serine (Fig. 6 *E* and *F*; $\langle \mathrm{Tsr} \rangle_{\mathrm{batch}} = 29.6 \pm 2.9 \mu m^{-2}$ and $\langle \mathrm{Tsr} \rangle_{\mathrm{wave}} = 53.6 \pm 6.5 \mu m^{-2}$).

While the distribution of Tsr changed significantly depending on the attractant the population was chasing (*SI Appendix*, Fig. S12 for a direct comparison), the distributions of TB were similar across attractants, with only a mild adjustment in serine (*SI Appendix*, Fig. S13), suggesting that adaptation of these two traits is nearly independent.

To confirm that the shift in the distribution of Tsr levels was not due to gene regulation, we employed an analogous strategy to the one described above for CheY and CheZ (*SI Appendix*, Fig. S7*A*), here using a nonmotile strain expressing fluorescently labeled Tsr from its native locus (*SI Appendix*, Fig. S14*A*). There were no differences in the Tsr levels between nonmotile cells harvested at the migrating edge and at the center of the plate, suggesting that *tsr* gene expression changes negligibly during collective migration (*SI Appendix*, Fig. S14 *B* and *C*). Tsr levels were not regulated by serine or aspartate consumption (when these amino acids were present in batch cultures at the same concentrations as in the swim plates) (*SI Appendix*, Fig. S15), nor were TB distributions (*SI Appendix*, Fig. S16). This further indicated that the receptor enrichment that we measured after migration on swim plates was not caused by altered gene expression or metabolic effects due to the presence of amino acids.

Taken together, these observations demonstrated that adaptation by collective migration generalizes to sensory phenotypes: Migrating populations nongenetically adapted their distributions of receptor abundances, depending on the attractants they were chasing. Thus, collective migration combined with growth can enrich for multiple, continuous phenotypic traits and nongenetically adapt migrating populations to diverse environmental conditions.

Discussion

Here, we investigated how a population of cells adapts its distribution of phenotypes to migrate effectively in multiple environments. We found that migrating populations of *E. coli* can tune their distributions of swimming behaviors and sensing capabilities based on the physical and chemical properties of their environment. This tuning occurs dynamically and is explained by a model in which loss of low-performing chemotaxis phenotypes from a migrating front (15) balances the production of new phenotypes by growth (18, 25). This mechanism, which we demonstrated in multiple *E. coli* strains, can act on preexisting variability in gene expression but does not require de novo changes in gene expression or mutations. By rapidly and reversibly enriching for fitter individuals based on the demands of the current environment, this mechanism increases the population's expansion speed across a wide variety of potential environments.

We examined two phenotypes that impact chemotaxis performance: tumble bias and receptor abundance. In liquid, low tumble bias cells are known to climb a fixed gradient faster (17). Consistent with this WT RP437 populations enriched for low-TB cells when migrating in liquid. When migrating on agarose, however, the TB distribution did not change from the standing batch distribution. Furthermore, both CheZ-inducible populations, with high or low initial mean TB, shifted toward the standing batch distribution of the WT RP437 (*SI Appendix*, Fig. S2). This suggests that the standing batch TB distribution of WT RP437 is already adapted for navigation in agar/agarose. Indeed, RP437 is a standard laboratory strain that has been used to study motility for decades (39, 42) and was originally selected for motility on agar swim plates. In all the strains we tested, the tumble bias distribution when migrating in liquid was enriched for lower TB cells than when migrating on agarose (Fig. 5 *A* and *B* and *SI Appendix*, Fig. S9). This is consistent with previous findings that tumbling slows migration in liquid (17, 29), but that tumbles are needed to escape traps in porous environments (23, 43, 44). More broadly, we expect that any phenotypic trait that contributes to chemotaxis performance can be enriched during collective migration. For example, standing variation in FliC expression can lead to variation in swimming speed (45), and migrating fronts have been shown to be enriched with cells with higher FliC expression (21). This observation could be due to adaptation by collective migration, possibly in tandem with gene regulation. Finally, it is always possible for one of the countless strains of bacteria in nature to encounter an environment in which its phenotype composition is poorly adapted. In these cases, we expect nongenetic adaptation to have large effects on its traveling phenotype distribution.

We also found that the adapted TB distributions relaxed back to the batch culture distribution in about two generations, indicating some degree of nongenetic inheritance. This is consistent with a previous study which showed that swimming traits of individual *E. coli* cells are partially and nongenetically inherited across multiple generations (25). While nongenetic inheritance of chemotactic traits (25), and other traits like antibiotic resistance (46), sporulation (47), iron metabolism (48) were studied previously, the molecular mechanism of how these traits are inherited remains to be explored further. Indeed, nongenetic inheritance of chemotactic traits may involve partitioning of chemoreceptors, flagellar components, and other regulatory elements from the mother to daughter cells during cell division.

Recent research emphasizes the crucial role of emergent spatial structures during collective migration in enhancing genetic diversity within bacterial communities (49). In traditional well-mixed environments, resource competition leads to the extinction of species with lower relative growth fitness (50). However, during collective migration, species with lower relative growth fitness can coexist by competing for spatial territories rather than resources (4, 49), and avoid extinction by colonizing specific habitats within the migrating colony. Furthermore, recent experiments demonstrate the evolution of mutants with different navigation capabilities from isogenic migrating populations (4), suggesting that the emergent spatial organization of phenotypes could contribute to genetic diversity (15, 20, 51, 52). Together with our observation that environment determines the specific distribution of phenotypes that is enriched, these results suggest that relative spatial arrangements of phenotypes within migrating groups may play an important role in ecoevolutionary dynamics.

Collective migration is not exclusive to bacteria; it also occurs in eukaryotic systems where cells consume or degrade attractants to form and chase self-generated gradients, a mechanism observed in various contexts including cancer and development (53, 54). Some examples are the migration of lateral line of zebrafish embryos (55), neural crest cells in *Xenopus laevis* (56), and melanoma cells (57). The tuning of phenotypic distributions during collective migration only requires that some cells, due to their specific traits, are more adept at navigating than others, therefore creating a "leader–follower" structure. Thus, adaptation by collective migration may be a general strategy for cell populations to colonize diverse environments effectively.

Adaptation mechanisms such as stochastic switching (7, 9, 58) and regulating gene expression are fast (~1 generation) but are limited to the adaptation of a few phenotypic traits and often require dedicated pathways to implement. Adaptation by genetic mutations avoids these limitations but is slow (~10 generations) (4–6). In contrast, standing variation in numerous phenotypic traits among individual cells is ubiquitous. Our findings demonstrate that when collective behaviors create selection pressures

which shape that variation, cell populations can reversibly adapt multiple traits with a level of speed and flexibility that is difficult to achieve via classical mechanisms.

Methods

Strains, Media, and Growth Conditions. Most experiments were performed with *E. coli* K12 RP437 and MG1655 derivatives. Other strains used in this study are *E. coli* HE205, AW405, and wild-isolate TW09231 (*Escherichia sp.* TW09231). To tune tumble bias distributions, we utilized *E. coli* RP437 Δ*cheZ* and HE205 Δ*cheZ* strains that carry an aTc-inducible cassette of *cheZ* that is integrated in the chromosome at the *attB* site (RP437 Δ*cheZ pTet-cheZ* and HE205 Δ*cheZ pTet-cheZ*). To measure single-cell Tsr receptor abundances, we utilized an *E. coli* MG1655 *ΔfliC:FLP* mutant (gift from Victor Sourjik) that has *tsr* translationally fused with monomeric YFP (A206K) on its native chromosomal locus (MG1655 Δ*fliC:FLP, tsr-mYFP*). To modulate motility in the previous strain, we transformed an arabinose-inducible plasmid expressing WT FliC (*pBad-fliC*, gift from Howard Berg) into MG1655 Δ*fliC:FLP, tsr-mYFP*, and induced it with 0.005% w/v arabinose. RP437 Δ*fliC* with CheY and CheZ translationally fused with mRFP and mYFP, respectively on their native chromosomal loci (RP437 Δ*fliC cheY-mRFP and cheZ-mYFP*) was used as a biosensor to measure expression of the *cheY* and *cheZ* genes in the swim plate assays. MG1655 Δ*fliC:FLP*, *tar-mCherry, tsr-mYFP*, was used as a biosensor to measure expression of the *tsr* gene. To insert genes on the native loci of the *E. Coli* chromosome, we employed the phage λ Red recombination system.

RP437-derived strains were stored as −80 °C freezer DMSO-based stocks, and MG1655-derived strains were stored as glycerol-based stocks at the same temperature. M9 buffer supplemented with casamino acids, glycerol, and $MgSO_4$ (1x M9 salts, 0.4% v/v glycerol, 0.1% v/v casamino acids, 1 mM $MgSO_4$; pH 7.0) were used to grow RP437-derived strains, AW405, and TW09231. H1 minimal salts medium (MMH1: 50 mM KPO_4, 0.5 mM $MgSO_4$, 7.6 mM $(NH_4)_2SO_4$, 1.25 μM $Fe_2(SO_4)_3$; pH 7.0) supplemented with 0.5% v/v glycerol and 0.01% w/v thiamine hydrochloride was used to grow MG1655-derived strains. MOPS glycerol media (8.37 g/L MOPS adjusted to pH 7.0 with KOH, 0.712 g/L tricine adjusted to pH 7.0 with KOH, 0.00278 g/L $FeSO_4$ $7H_2O$, 0.0481 g/L K_2SO_4, 0.0000555 g/L $CaCl_2$, 0.106 g/L $MgCl_2$ $6H_2O$, 2.91 g/L NaCl, 0.0230 g/L K_2PO_4, 2 mM NH_4Cl, and 4 mL/L glycerol) were used to grow HE205 derived strains. To grow overnight cultures, small inoculants from the freezer stocks were added into test tubes containing 2 mL of media (with appropriate concentrations of inducers and antibiotics) in a shaking incubator at 30 °C rotating at 250 RPM. To grow day cultures for cell tracking experiments, RP437-derived strain overnight cultures were diluted 100-fold and regrown in 5 mL of the appropriate media until exponential phase (OD_{600} = 0.20). For receptor quantification experiments, MG1655-derived strains were diluted 200-fold and regrown in 10 mL of the appropriate media until exponential phase (OD_{600} = 0.30). For cell tracking experiments, chemotaxis buffer (1× M9 buffer, 0.4% v/v glycerol, 0.010 mM methionine, 0.1 mM EDTA, and 0.1% v/v PVP-40) was used to wash and dilute cells. For receptor quantification experiments, minimal chemotaxis buffer (10 mM KPO_4 and 0.1 mM EDTA; pH 7.0) was used to wash and dilute cells. For the TB measurements in batch cultures, RP437 Δ*cheZ pTet-cheZ* cells were grown in media supplemented with aTc that was aged for 15 h.

Growth Rates Measurements. Growth measurements were done using a microplate reader (BioTek Epoch 2 microplate spectrophotometer). Overnight cultures were diluted 100-fold into fresh media supplemented with appropriate inducer concentrations. 200 μL of diluted cells were aliquoted into each well of polystyrene 96-well plates (Falcon 96-wells REF 353072), and the plates were loaded into the plate reader. The plates were incubated at 30 °C while continuously shaking linearly at 567 cpm. The OD_{600} of each well was measured every 7 min for 36 h. To extract the growth rates of each sample, the slopes of the linear region (at the mid-exponential growth phases) of the natural log of OD_{600} versus time (hours) curves were calculated.

Formation of Propagating Waves and Expansion Speed Measurements Using Swim Plate and Capillary Tube Assays. For the swim plate assay, 3 μL of cells in exponential phase was inoculated at the center of semisolid agarose plates for RP437-derived strains or 10 μL of cells in exponential phase for MG1655-derived strains. For RP437-derived strains, the semisolid agarose plates were made using M9-based media, as described above, supplemented with 0.14% agarose (American Bioanalytical Agarose GPG/LE) and appropriate concentrations of aTc. Similarly, for MG1655-derived strains, the semisolid agarose plates were made using H1 minimal media, as described above, supplemented with 0.14% agarose. The plates were incubated at 30 °C for 15 h (RP437-derived strains) or at 33.5 °C for 48 h (MG1655-derived strains). The edges of the migrating colonies were picked using pipette tips and diluted into chemotaxis buffer (for RP437-derived strains) or minimal chemotaxis buffer (for MG1655-derived strains) for subsequent tracking and imaging analyses. To measure the expansion speeds of bacterial populations in swim plates, images were taken with a Canon DS126291 camera every 30 min. The diameters of the expansion rings as a function of time and expansion speeds were extracted from the images using a customized MATLAB code.

For the capillary tube assay, the protocol was adapted from previous work (14). Overnight cultures were inoculated 100-fold into 5 mL of media with appropriate inducers and grown at 30 °C until OD_{600} = 0.2. Cells were concentrated to an OD_{600} = 6. A 12-inch capillary tube was filled with growth media (M9 glycerol with casamino acids, $MgSO_4$, and PVP-40) and 6-h aged aTc, and one side of the tube was plugged by stabbing the tube into a plate filled with solidified agar (1.5% agar in distilled water). The concentrated cell mixture was filled on the other side of the tube using a 1 mL syringe, and another agar plug was added into that side. Both sides of the tube were then plugged with clay. The tubes are incubated horizontally at 30 °C for 9 h. To isolate the wave, a 3-cm section of the tube that contained the wave was fractionated, and the mixture inside the 3-cm section was diluted into chemotaxis buffer for subsequent tracking analysis. To measure the expansion speeds of bacterial populations in capillary tubes, images were taken with a Canon DS126291 camera every 10 min. Positions of the populations as a function of time and expansion speeds were extracted from images using ImageJ.

Microfluidic Device Preparation. To track single-cell swimming behavior, we utilized a rectangular channel microfluidic device (0.5 mm wide, 30 mm long, and 60 μm deep). The device was constructed from PDMS with standard lithography methods. To cast the device, a preprepared mold was coated with a 5-mm thick layer of degassed 10:1 PDMS-to-curing agent mixture (Sylgard 184, Dow Chemical). The mold was then baked at 70 °C for 12 h. Devices were cut out of the mold, and a hole was punched using a 20-gauge blunt-tip needle on each side of the channel. The device was rinsed with isopropanol, methanol, and water. A 22 mm × 50 mm glass coverslip was rinsed with acetone, isopropanol, methanol, and water. The coverslip and device were then treated inside a plasma cleaner for 1 min and bonded together. The bonded device was heated at 80 °C for 15 min and cooled to room temperature before cells were injected inside.

Tracking Single Cells and Tumble Detection. Washed cells were diluted with chemotaxis buffer to an OD_{600} = 0.0005. The diluted mixture was injected inside the microfluidic device using a 1 mL syringe. To prevent evaporation, holes on both sides of the microfluidic device were taped. The device was placed on an inverted microscope (Nikon Eclipse Ti-U) equipped with a custom environmental chamber (50% humidity and 30 °C). A custom MATLAB script was used to record 3-min phase contrast videos at 4X magnification and 20 frames-per-second. Video recordings were stored as .bin files.

Custom MATLAB code was used to detect tumble and extract tumble bias of single cells, as previously described (59). Only trajectories longer than 10 s were considered for analysis. Each tumble bias distribution was generated from four 3-min videos that contained ~1,000 total trajectories. The analyzed trajectory data were stored as .mat files.

Measuring the Time Scales of Relaxation of TB Distribution to the Standing Batch Distribution. *E. coli* RP437 or HE205 were grown to early-exponential phase (OD_{600} = 0.2) and put to migrate in capillary tubes for 9 h, as mentioned above. The sections of the capillary tubes containing the migrating bacterial populations were fractioned, and the cells were added into 1 mL of growth media. For every 15- or 30-min during growth in the batch cultures, the TB distributions of the populations were measured. The mean of TB distributions normalized by the trajectory lengths were determined for each time points.

The equation to model for the relaxation of mean TB is:

$$TB(t) = TB_{batch} - \left(TB_{batch} - TB_0\right)e^{-\frac{t}{\tau}},$$

where $TB(t)$ is the mean TB over time, TB_{batch} is the mean TB of the batch culture, TB_0 is the mean TB during collective migration in the capillary tubes, and τ is the relaxation timescale. To estimate τ, we fitted the means of the mean TBs across replicates and the SE of the means across replicates to the equation using maximum likelihood estimation. To estimate the error of τ, we sampled the posterior distribution using Markov Chain Monte Carlo to get 100 sampled parameter values and then calculated the standard deviation of those samples.

Protein Expression Measurements in Swim Plates. Nonmotile MG1655-derived cells expressing labeled Tsr or nonmotile RP437-derived cells expressing labeled CheY and CheZ used as biosensors for gene expression were grown as described above. Subsequently, cells were mixed with the appropriate media and 0.14% liquefied agarose to a final $OD_{600} = 0.01$. Swim plates were left to solidify at room temperature for 2 to 3 h, and afterward, 10 μL of $OD_{600} = 0.01$ motile WT MG1655 (labeled Tsr experiments) or motile WT RP437 (labeled CheY and CheZ experiments) cells were inoculated in the center of the plate. The motile population of cells shapes the gradient of the plate and ensures that the nonmotile biosensor strain experiences the same local environment as motile cells. After a colony of migrating cells has formed, cells from the center and the edge of the colony are picked and diluted into minimal chemotaxis buffer for subsequent imaging.

Single-Cell Protein Copy Number Quantification Using Fluorescent Microscopy. Washed cells were diluted 10-fold and plated on agarose pads (3% agarose in minimal chemotaxis buffer). The cell suspension was left to dry for 10 min, and cells were immediately imaged afterward. Imaging was performed using an inverted microscope (Nikon Eclipse Ti-E) equipped with an oil immersion 100× phase-contrast objective lens. To measure the fluorescence intensity of the strain expressing cheY-mRFP and cheZ-mYFP, fluorescent proteins were excited using a light-emitting diode illumination system (pE-4000, CoolLED). The RFP and YFP channels were imaged consecutively using a multiband filter (Semrock), and the fluorescence emissions were led into a 2-camera image splitter (TwinCam, Cairn), leading to two identical sCMOS cameras (ORCA-Flash4.0 V2, Hamamatsu). The same setup was used to measure the fluorescence intensity of the strain expressing Tsr-mYFP. In a typical experiment, 20 fields of view, containing approximately 1,000 cells in total, are imaged.

Fluorescent Image Analysis for Protein Copy Number Quantification. For each field of view, one phase contrast, one YFP, and one RFP channel images were acquired. Using a custom MATLAB script, images from the two cameras were aligned using an affine transformation, and cells were segmented on the phase-contrast channel using a modified Otsu algorithm. Then, the image background was subtracted from each image, and the fluorescent intensity of every cell was extracted. Finally, the area of each cell was calculated by fitting an ellipsoid. The fluorescent intensity of each cell was divided by the cell area as a measure of protein concentration.

Reproducibility and Statistical Analysis. All experiments reported in this work were repeated at least three times. All measurement values of TB, expansion speeds, growth rates, protein levels were reported as the average of the means of the distributions across biological replicates. Uncertainties in these average values were reported as the SD of the means of the distributions.

To construct the TB distributions, TB values were sorted into bins, and the probability densities were normalized by dividing the trajectory time within each bin by the total trajectory time. To represent the variations in TB distributions, the SEM TBs within each bin was calculated. Similarly, with the Tsr intensity distribution, single-cell Tsr intensities were sorted into bins, and the probability density in each bin was calculated. The variations in Tsr intensity distributions are represented as the SEM intensities within each bin.

To construct the fold-enrichment curve, the probability density values of each TB or Tsr intensity bins observed in the distributions during collective migration were divided by the values observed in batch cultures. Variations in fold-enrichments are represented as the SEM fold-enrichment values within each bin.

To determine statistical significance between TB and protein level distributions, the two-sided t test was performed on the mean values. Similarly, the two-sided t test was performed to determine significance of growth rates and expansion speeds between experiments (throughout, $***P < 0.0005$, $**P < 0.005$, $*P < 0.05$, and n.s. = not significant).

Data, Materials, and Software Availability. Non-genetic adaptation by collective migration/Analysis Code data have been deposited in Dryad/Github (https://doi.org/10.5061/dryad.ksn02v7fd; http://github.com/emonetlab) (60, 61).

ACKNOWLEDGMENTS. We thank Jing Yan, Amir Pahlavan, Jeremy Moore, Jyot Antani, Karen Fahrner, Kiri Choi, and Gustavo Santana for useful discussions. We thank Simone Boskamp for assistance with cloning and Cherin Mohamed for assistance with experiments. We thank Jonas Cremer and Terrence Hwa for providing *E. coli* HE205 wild-type strain. We thank Victor Sourjik and Howard Berg for providing plasmids and strains that were important for this work. This work was supported by NIH awards R01GM138533 and R01GM106189 and by the Alfred P. Sloan Foundation award 699G-2023-19668. Lam Vo is supported by NIH F31GM149174-01.

Author affiliations: [a]Department of Molecular, Cellular, and Developmental Biology, Yale University, New Haven, CT 06511; [b]Quantitative Biology Institute, Yale University, New Haven, CT 06511; [c]Center for Living Systems, AMOLF Institute, Amsterdam 1098 XG, The Netherlands; [d]Center for Computational Biology, Flatiron Institute, New York City, NY 10010; [e]Departments of Medicine and Microbial Pathogenesis, Yale University, New Haven, CT 06511; and [f]Department of Physics, Yale University, New Haven, CT 06511

1. B. K. Chan *et al.*, Phage selection restores antibiotic sensitivity in MDR Pseudomonas aeruginosa. *Sci. Rep.* **6**, 26717 (2016), 10.1038/srep26717.
2. K. Poole, Outer membranes and efflux: The path to multidrug resistance in Gram-negative bacteria. *Curr. Pharm. Biotechnol.* **3**, 77–98 (2002), 10.2174/1389201023378454.
3. M. W. Schmitt, L. A. Loeb, J. J. Salk, The influence of subclonal resistance mutations on targeted cancer therapy. *Nat. Rev. Clin. Oncol.* **13**, 335–347 (2016), 10.1038/nrclinonc.2015.175.
4. W. Liu, J. Cremer, D. Li, T. Hwa, C. Liu, An evolutionarily stable strategy to colonize spatially extended habitats. *Nature* **575**, 664–668 (2019), 10.1038/s41586-019-1734-x.
5. D. T. Fraebel *et al.*, Environment determines evolutionary trajectory in a constrained phenotypic space. *Elife* **6**, e24669 (2017), 10.7554/eLife.24669.
6. B. Ni *et al.*, Evolutionary remodeling of bacterial motility checkpoint control. *Cell Rep.* **18**, 866–877 (2017), 10.1016/j.celrep.2016.12.088.
7. T. M. Norman, N. D. Lord, J. Paulsson, R. Losick, Stochastic switching of cell fate in microbes. *Annu. Rev. Microbiol.* **69**, 381–403 (2015), 10.1146/annurev-micro-091213-112852.
8. E. Kussell, S. Leibler, Phenotypic diversity, population growth, and information in fluctuating environments. *Science* **309**, 2075–2078 (2005), 10.1126/science.1114383.
9. N. Q. Balaban, J. Merrin, R. Chait, L. Kowalik, S. Leibler, Bacterial persistence as a phenotypic switch. *Science* **305**, 1622–1625 (2004), 10.1126/science.1099390.
10. E. Kussell, R. Kishony, N. Q. Balaban, S. Leibler, Bacterial persistence: A model of survival in changing environments. *Genetics* **169**, 1807–1814 (2005), 10.1534/genetics.104.035352.
11. T. K. Wood, S. J. Knabel, B. W. Kwan, Bacterial persister cell formation and dormancy. *Appl. Environ. Microbiol.* **79**, 7116–7121 (2013), 10.1128/AEM.02636-13.
12. Y. Oren *et al.*, Cycling cancer persister cells arise from lineages with distinct programs. *Nature* **596**, 576–582 (2021), 10.1038/s41586-021-03796-6.
13. P. C. Bressloff, Stochastic switching in biology: From genotype to phenotype. *J. Phys. A: Math. Theor.* **50**, 133001 (2017).
14. T. Tian, K. Burrage, Stochastic models for regulatory networks of the genetic toggle switch. *Proc. Natl. Acad. Sci. U.S.A.* **103**, 8372–8377 (2006), 10.1073/pnas.0507818103.
15. X. Fu *et al.*, Spatial self-organization resolves conflicts between individuality and collective migration. *Nat. Commun.* **9**, 2177 (2018), 10.1038/s41467-018-04539-4.
16. J. Adler, Chemotaxis in bacteria. *Science* **153**, 708–716 (1966), 10.1126/science.153.3737.708.
17. A. J. Waite *et al.*, Non-genetic diversity modulates population performance. *Mol. Syst. Biol.* **12**, 10 (2016).
18. H. H. Mattingly, T. Emonet, Collective behavior and nongenetic inheritance allow bacterial populations to adapt to changing environments. *Proc. Natl. Acad. Sci. U.S.A.* **119**, e2117377119 (2022), 10.1073/pnas.2117377119.
19. J. Wong-Ng, A. Celani, M. Vergassola, Exploring the function of bacterial chemotaxis. *Curr. Opin. Microbiol.* **45**, 16–21 (2018), 10.1016/j.mib.2018.01.010.
20. J. Cremer *et al.*, Chemotaxis as a navigation strategy to boost range expansion. *Nature* **575**, 658–663 (2019), 10.1038/s41586-019-1733-y.
21. D. A. Koster, A. Mayo, A. Bren, U. Alon, Surface growth of a motile bacterial population resembles growth in a chemostat. *J. Mol. Biol.* **424**, 180–191 (2012), 10.1016/j.jmb.2012.09.005.
22. H. Zheng *et al.*, Interrogating the Escherichia coli cell cycle by cell dimension perturbations. *Proc. Natl. Acad. Sci. U.S.A.* **113**, 15000–15005 (2016), 10.1073/pnas.1617932114.
23. A. J. Wolfe, H. C. Berg, Migration of bacteria in semisolid agar. *Proc. Natl. Acad. Sci. U.S.A.* **86**, 6973–6977 (1989), 10.1073/pnas.86.18.6973.
24. J. F. Staropoli, U. Alon, Computerized analysis of chemotaxis at different stages of bacterial growth. *Biophys. J.* **78**, 513–519 (2000), 10.1016/S0006-3495(00)76613-6.
25. M. Pleska, D. Jordan, Z. Frentz, B. Xue, S. Leibler, Nongenetic individuality, changeability, and inheritance in bacterial behavior. *Proc. Natl. Acad. Sci. U.S.A.* **118**, e2023322118 (2021), 10.1073/pnas.2023322118.
26. N. V. Vorobyeva, M. Sherman, A. N. Glagolev, Bacterial chemotaxis controls the catabolite repression of flagellar biogenesis. *FEBS Lett.* **143**, 233–236 (1982), 10.1016/0014-5793(82)80106-3.
27. M. Scott, T. Hwa, Shaping bacterial gene expression by physiological and proteome allocation constraints. *Nat. Rev. Microbiol.* **21**, 327–342 (2023), 10.1038/s41579-022-00818-6.
28. N. A. Licata, B. Mohari, C. Fuqua, S. Setayeshgar, Diffusion of bacterial cells in porous media. *Biophys. J.* **110**, 247–257 (2016), 10.1016/j.bpj.2015.09.035.

29. Y. S. Dufour, X. Fu, L. Hernandez-Nunez, T. Emonet, Limits of feedback control in bacterial chemotaxis. *PLoS Comput. Biol.* **10**, e1003694 (2014), 10.1371/journal.pcbi.1003694.
30. C. S. Barker, B. M. Pruss, P. Matsumura, Increased motility of Escherichia coli by insertion sequence element integration into the regulatory region of the flhD operon. *J. Bacteriol.* **186**, 7529–7537 (2004), 10.1128/JB.186.22.7529-7537.2004.
31. C. Luo *et al.*, Genome sequencing of environmental Escherichia coli expands understanding of the ecology and speciation of the model bacterial species. *Proc. Natl. Acad. Sci. U.S.A.* **108**, 7200–7205 (2011), 10.1073/pnas.1015622108.
32. Y. Tu, T. S. Shimizu, H. C. Berg, Modeling the chemotactic response of Escherichia coli to time-varying stimuli. *Proc. Natl. Acad. Sci. U.S.A.* **105**, 14855–14860 (2008), 10.1073/pnas.0807569105.
33. J. M. Keegstra *et al.*, Phenotypic diversity and temporal variability in a bacterial signaling network revealed by single-cell FRET. *Elife* **6**, e27455 (2017), 10.7554/eLife.27455.
34. H. Salman, A. Libchaber, A concentration-dependent switch in the bacterial response to temperature. *Nat. Cell Biol.* **9**, 1098–1100 (2007), 10.1038/ncb1632.
35. Y. Yang *et al.*, Relation between chemotaxis and consumption of amino acids in bacteria. *Mol. Microbiol.* **96**, 1272–1282 (2015), 10.1111/mmi.13006.
36. M. Li, G. L. Hazelbauer, Cellular stoichiometry of the components of the chemotaxis signaling complex. *J. Bacteriol.* **186**, 3687–3694 (2004), 10.1128/JB.186.12.3687-3694.2004.
37. F. R. Blattner *et al.*, The complete genome sequence of Escherichia coli K-12. *Science* **277**, 1453–1462 (1997), 10.1126/science.277.5331.1453.
38. J. Adler, G. L. Hazelbauer, M. M. Dahl, Chemotaxis toward sugars in Escherichia coli. *J. Bacteriol.* **115**, 824–847 (1973), 10.1128/jb.115.3.824-847.1973.
39. J. S. Parkinson, S. E. Houts, Isolation and behavior of Escherichia coli deletion mutants lacking chemotaxis functions. *J. Bacteriol.* **151**, 106–113 (1982), 10.1128/jb.151.1.106-113.1982.
40. R. G. Endres, N. S. Wingreen, Precise adaptation in bacterial chemotaxis through "assistance neighborhoods". *Proc. Natl. Acad. Sci. U.S.A.* **103**, 13040–13044 (2006), 10.1073/pnas.0603101103.
41. V. Sourjik, Receptor clustering and signal processing in E. coli chemotaxis. *Trends Microbiol.* **12**, 569–576 (2004), 10.1016/j.tim.2004.10.003.
42. J. S. Parkinson, cheA, cheB, and cheC genes of Escherichia coli and their role in chemotaxis. *J. Bacteriol.* **126**, 758–770 (1976), 10.1128/jb.126.2.758-770.1976.
43. T. Bhattacharjee, S. S. Datta, Bacterial hopping and trapping in porous media. *Nat. Commun.* **10**, 2075 (2019), 10.1038/s41467-019-10115-1.
44. C. Kurzthaler *et al.*, A geometric criterion for the optimal spreading of active polymers in porous media. *Nat. Commun.* **12**, 7088 (2021), 10.1038/s41467-021-26942-0.
45. I. Lisevich, R. Colin, H. Y. Yang, B. Ni, V. Sourjik, Physics and physiology determine strategies of bacterial investment in flagellar motility. bioXriv [Preprint] (2024), 10.1101/2024.03.30.587422.
46. A. Joers, T. Tenson, Growth resumption from stationary phase reveals memory in Escherichia coli cultures. *Sci. Rep.* **6**, 24055 (2016), 10.1038/srep24055.
47. J. W. Veening *et al.*, Bet-hedging and epigenetic inheritance in bacterial cell development. *Proc. Natl. Acad. Sci. U.S.A.* **105**, 4393–4398 (2008), 10.1073/pnas.0700463105.
48. S. Bhattacharyya *et al.*, A heritable iron memory enables decision-making in Escherichia coli. *Proc. Natl. Acad. Sci. U.S.A.* **120**, e2309082120 (2023), 10.1073/pnas.2309082120.
49. S. Gude *et al.*, Bacterial coexistence driven by motility and spatial competition. *Nature* **578**, 588–592 (2020), 10.1038/s41586-020-2033-2.
50. J. E. Goldford *et al.*, Emergent simplicity in microbial community assembly. *Science* **361**, 469–474 (2018), 10.1126/science.aat1168.
51. Y. Bai *et al.*, Spatial modulation of individual behaviors enables an ordered structure of diverse phenotypes during bacterial group migration. *Elife* **10**, e67316 (2021), 10.7554/eLife.67316.
52. W. Zuo, Y. Wu, Dynamic motility selection drives population segregation in a bacterial swarm. *Proc. Natl. Acad. Sci. U.S.A.* **117**, 4693–4700 (2020), 10.1073/pnas.1917789117.
53. G. Venkiteswaran *et al.*, Generation and dynamics of an endogenous, self-generated signaling gradient across a migrating tissue. *Cell* **155**, 674–687 (2013), 10.1016/j.cell.2013.09.046.
54. C. Scherber *et al.*, Epithelial cell guidance by self-generated EGF gradients. *Integr. Biol. (Camb.)* **4**, 259–269 (2012), 10.1039/c2ib00106c.
55. N. B. David *et al.*, Molecular basis of cell migration in the fish lateral line: Role of the chemokine receptor CXCR4 and of its ligand, SDF1. *Proc. Natl. Acad. Sci. U.S.A.* **99**, 16297–16302 (2002), 10.1073/pnas.252339399.
56. E. Theveneau, R. Mayor, Neural crest delamination and migration: From epithelium-to-mesenchyme transition to collective cell migration. *Dev. Biol.* **366**, 34–54 (2012), 10.1016/j.ydbio.2011.12.041.
57. A. J. Muinonen-Martin *et al.*, Melanoma cells break down LPA to establish local gradients that drive chemotactic dispersal. *PLoS Biol.* **12**, e1001966 (2014), 10.1371/journal.pbio.1001966.
58. M. Acar, J. T. Mettetal, A. van Oudenaarden, Stochastic switching as a survival strategy in fluctuating environments. *Nat. Genet.* **40**, 471–475 (2008), 10.1038/ng.110.
59. H. H. Mattingly, K. Kamino, B. B. Machta, T. Emonet, Escherichia coli chemotaxis is information limited. *Nat. Phys.* **17**, 1426–1431 (2021), 10.1038/s41567-021-01380-3.
60. L. Vo *et al.*, Non-genetic adaptation by collective migration, experimental data. Dryad. https://doi.org/10.5061/dryad.ksn02v7fd. Accessed 4 February 2025.
61. L. Vo *et al.*, Non-genetic adaptation by collective migration, analysis code. Github. http://github.com/emonetlab. Accessed 4 February 2025.